

Thermodynamic design, evaluation, and optimization of a novel quadruple generation system combined of a fuel cell, an absorption refrigeration cycle, and an electrolyzer

Leyla Khani¹ | Mahsa Mohammadpour¹ | Mousa Mohammadpourfard¹  |
Saeed Zeinali Heris¹  | Gülden Gökçen Akkurt²

¹Faculty of Chemical and Petroleum Engineering, University of Tabriz, Tabriz, Iran

²Department of Energy Systems Engineering, Izmir Institute of Technology, Izmir, Turkey

Correspondence

Mousa Mohammadpourfard, Faculty of Chemical and Petroleum Engineering, University of Tabriz, Tabriz, Iran.
Email: mohammadpour@tabrizu.ac.ir

Summary

In this article, a solid oxide fuel cell system is combined with a generator absorber heat exchanger absorption refrigeration cycle and a proton exchange membrane electrolyzer unit to use most of the fuel energy and recover waste heat and material. This quadruple-generation system produces electric power, refrigeration, heating, and hydrogen from natural gas as the primary energy source for the system. The thermodynamic and environmental performances of the system are studied comprehensively to identify the effects of the key operating parameters on the system operation. The results show that as fuel cell current density increases from 2000 to 8000 A/m²; the system energy and exergy efficiencies decrease by nearly 20%, but the unit carbon dioxide emission increases by 30.38%. Also, the energy and exergy efficiencies are maximized, and the unit carbon dioxide emission is minimized at a specified value of fuel utilization factor. Additionally, increasing the steam to carbon ratio has a damaging effect on the system efficiencies but leads to higher unit carbon dioxide emission. Then, the genetic algorithm is applied to optimize the condition, so the highest exergy efficiency is attainable. The optimization results demonstrate that an exergy efficiency as high as 0.6443 is achievable.

KEYWORDS

absorption refrigeration, electrolyzer, multigeneration, solid oxide fuel cell, thermodynamic analysis

1 | INTRODUCTION

Nowadays, energy is an indispensable part of economic and human life development. It is predicted that energy consumption will rise tremendously. Fossil fuels are the primary energy resource worldwide, but they have some significant disadvantages. First, they are practically non-renewable and limited. Second, they contribute to environmental pollution and its side effects like health problems, global warming, and climate change. Third,

conventional combustion-based power plants are ineffective; they can convert only 40% of the fuel's latent energy to electrical power. Hence, researchers devise new solutions to extract the most of fossil fuels' energy cleanly, safely, and economically.

The first proposed solution is using new energy conversion methods like electrochemical reactions to directly convert fuel's chemical energy into electricity through the transfer of electrons and charges of substances. It is in contrast to combustion (chemical reaction), in which,

fuel burns to produce heat, and in another step, the heat changes to mechanical and electrical power. Fuel cells are such devices to carry out electrochemical reactions continuously. They have many advantages such as low environmental effects, high energy efficiency, fuel variety, capacity and application diversity, controllable operation, size management, and few moving parts. Also, the excess heat of high-temperature fuel cells can be used as an energy source for other low/mid-temperature systems.¹ In this case, the developed system can produce two or more kinds of products from only one fuel resource. The second solution researchers have put forward is the usage of system's waste energy or stream in other cycles and design co/tri/multigeneration systems to increase system outputs, efficiency, and profitability and reduce pollution.² Solid oxide fuel cell (SOFC) is a high-temperature fuel cell that many researchers have considered in various integrated schemes, such as cogeneration, trigeneration, or multigeneration systems.³

Jia et al⁴ studied the performance of a new combination of a SOFC, a biomass gasification unit, a gas turbine, and an absorption chiller to produce power, heating, and cooling. They concluded that increasing the air flowrate into the biomass gasifier and decreasing biomass moisture have positive effects on the system efficiency. Habibollahzade et al⁵ proposed four schemes that generate power, heating, cooling, and hydrogen or methane. To achieve this goal, they considered a biomass-based SOFC as the main subsystem and added a double-effect absorption refrigeration cycle, a thermoelectric generator, a solid oxide electrolyzer, and a fuel synthesis unit as the helping components. They claimed that the combined SOFC-absorption chiller has the highest net power and exergy efficiency with the lowest production cost. Hosseinpour et al⁶ presented a new system of wood-fed biomass, an SOFC, and a Goswami cycle. Goswami cycle produced extra power from the waste heat of SOFC. Their obtained results showed that with higher turbine inlet pressure and SOFC inlet temperature, the rate of produced power and exergy efficiency reached their maximum values at 481.6 kW, 60.2%, and 34.7%, respectively. Tian et al⁷ proposed a new triple system, comprising a solid oxide, an organic Rankine cycle, an ammonia-water absorption chiller, and a carbon dioxide storage system. Their results indicated that the system electrical and exergy efficiencies were 52.83% and 59.966%, respectively. You et al⁸ analyzed exergy, economic, environmental performances and performed a multiobjective optimization of a micro polygeneration system for power, cooling, heating, and freshwater generation. The system included a SOFC, a gas microturbine, a multifunction desalination unit, an organic steam refrigerator, and a heat exchanger. They obtained the system electrical, exergy, and overall

energy efficiencies as 62.40%, 64.70%, and 67.13%, respectively. Ebrahimi and Moradpoor⁹ studied a new combination of a SOFC, a gas turbine, and an organic Rankine cycle. They reported that fuel-saving ratio in micro-scale generation was 45%. Gholamian et al¹⁰ studied the waste heat recovery of SOFC-gas turbine by either Kalina or organic Rankine cycles. They concluded that the system efficiency is 62.4%. Chitgar et al¹¹ presented a parametric study of a new gas turbine-SOFC system for the electricity, hydrogen, and water generation. The total cost of the products and the exergy efficiency were \$34.5/GJ and 54.2% at the optimum point, respectively. Atsonios et al¹² proposed a new concept of multigeneration liquid natural gas-based power plants for electricity, cooling, and water production in island systems. Their simulation results indicated that the SOFC-gas turbine combined power plant was the best solution from the energy efficiency viewpoint. Also, the multieffect distillation unit based on waste heat recovery was a good option for producing freshwater with nearly no energy cost. Khani et al¹³ proposed a multiproduction system composed of a gas turbine, a hydrogen-fed SOFC, and an absorption refrigeration cycle. The system performance was investigated and optimized to determine maximum exergy efficiency and minimum cost. Zhao et al¹⁴ suggested a composite cooling, heating, and energy generation system integrated with a solid oxide combustion cell and a lithium bromide-water absorption chiller. They found that the overall electrical system efficiencies could be almost 70% and 90%, respectively. Reyhani et al¹⁵ presented three combinations of SOFC-based multigeneration systems: SOFC-gas turbine, SOFC-gas turbine-steam turbine, and SOFC-gas turbine-multieffect distillation. The results showed that the optimal number of fuel cells for SOFC-gas turbine, SOFC-gas turbine-steam turbine, and SOFC-gas turbine-multieffect distillation schemes were 2300, 1700, and 600, respectively. Ozcan et al¹⁶ performed thermodynamic analysis of a modified internal reforming solid oxide fuel system using three different gaseous products. It was revealed that efficiency could rise by 54% with the proposed settings. Peng et al¹⁷ studied exergy, energy, and thermodynamic performance of a system combining a SOFC, a steam power turbine, a concentrating solar collector, and a chiller. They performed a parametric study to investigate the effect on their system of various variables. Akrami et al¹⁸ introduced and analyzed a solar-based energy system from the exergy and exergoeconomic viewpoints. The proposed system was economically viable at a unit cost of about \$4.617/GJ of generated power and a unit cost of refrigeration of about \$299.3/GJ daily. Sadeghi et al¹⁹ proposed a trigeneration fuel cell-based system, including an absorption refrigeration system and an additional heat exchanger. Their

system exergy efficiency and total product unit cost were estimated at 48.24% and \$25.94/GJ, respectively. Perna et al²⁰ proposed a combination of small-scale hydrogen, heating, and electricity production systems. The SOFC used ammonia to produce 100 kg hydrogen daily. Their results highlighted that high conversion of ammonia into hydrogen leads to low values of electrical and thermal efficiencies.

The above-mentioned published articles prove that SOFC-based multigeneration systems can be attractive options due to their high efficiency and low emission. Hence, more research and development are essential in this field. However, the feasibility of a SOFC-based quadruple generation system for simultaneous production of power, cooling, heating, and hydrogen has not been studied yet. Furthermore, the utilization of the oxygen generated in the proton exchange membrane electrolyzer (PEME) for burning anode outlet has not been evaluated. Also, material recovery in SOFC-based multigeneration systems is an important issue worth investigating. These necessities are addressed in this article. Following objectives are defined for this study:

- A novel power, heating, cooling, and hydrogen quadruple-generation system comprised of an SOFC, a generator absorber heat exchanger (GAX) absorption refrigeration cycle, and a proton exchange membrane electrolyzer is designed with the purpose of waste heat and material recovery, efficiency increase, and pollution reduction. The SOFC cathode outlet drives the GAX cycle to produce refrigeration. The energy and steam contents of the anode outlet support the PEME unit for hydrogen production.
- The possibility of material recovery, that is, steam for hydrogen production, PEME oxygen for burning anode outlet, and absorber cooling water for heat generation section, is evaluated in the system.
- The first and second laws of thermodynamics with mass conservation equations and necessary electrochemical relations are applied to components, sub-systems, and overall system as a steady-state control volume. Then, the energy and exergy efficiencies, the extent of irreversibilities, and the environmental criteria of the proposed system are determined. The obtained equations are solved using Engineering Equations Solver (EES) software.
- The effects of changing main operating parameters on the system thermodynamic and environmental performances are investigated through a parametric study.
- The genetic algorithm is used to define the system's optimal condition for maximum exergy efficiency.
- The main sources and extent of exergy destruction rate in the system are identified.

2 | SYSTEM DESCRIPTION

A schematic diagram of the proposed integrated SOFC-GAX-PEME system is depicted in Figure 1. The overall system combines the SOFC system as the power and heating production unit, the GAX cycle as the refrigeration unit, and the PEME system as the hydrogen generation unit. As represented in this figure, the SOFC sub-system is the topping unit. Its anode and cathode outlets are so hot that they can be heat sources for other cycles. The SOFC cathode outlet is sent to the GAX cycle, while the anode outlet is used in the heating production and PEME units. A detailed description of the quadruple-generation system is as follows:

- *SOFC sub-system:* The operating temperature of the SOFC stack is as high as around 800°C, so the inlet air, stream 5, and methane, stream 1, pass through compressors and heat exchangers and reach that temperature. Before entering the fuel cell stack, methane is mixed with a controlled fraction of the SOFC anode outlet (stream 11) in the mixer so that the necessary steam for the methane reforming reaction is provided. The internal reforming, water-gas shifting, and electrochemical reactions occur in the SOFC stack, and the electrical power is generated. Part of the power is used in the PEME unit to produce hydrogen, and the rest is sent to the electrical grid. Furthermore, the electrochemical reaction releases a significant amount of thermal energy, which compensates for the necessary heat of the reforming reaction and also leads to the higher temperature of the SOFC outlets, streams 8 and 9. The SOFC cathode outlet as stream 8 goes in HX2 to warm the inlet air and then in the generator of the GAX cycle as its high-temperature energy source. The anode outlet, stream 9, is divided into two parts; one section, which is stream 11, is sent back to the fuel cell stack after being mixed with the warm fresh fuel, stream 3; and the other part, named stream 10, is burned in the afterburner with the depleted oxygen from the PEME unit, stream 25, to eliminate the unreacted fuel and get more heat. The exhaust stream of the afterburner preheats the SOFC inlet fuel, stream 2, and the PEME outlet oxygen, stream 24. After that, it converts the GAX absorber outlet water, stream 42, into hot steam in the HX5. This steam can be used as a heating source for domestic applications. Finally, stream 17 condenses in the HX6, and its carbon dioxide content (stream 18) is separated from water. The water content goes to the PEME unit as stream 19 for hydrogen production.
- *PEME unit:* As shown in Figure 1, stream 19 enters the PEME unit. The water-splitting process takes place

- The cathode and anode outlets are at the same temperature as the fuel cell stack.
- Ambient conditions are $P_0 = 101.3$ kPa and $T_0 = 25^\circ\text{C}$
- Heat loss to the environment is negligible.
- Contact resistances are negligible in the SOFC stack.
- Potential and kinetic energy and exergy changes are ignored.
- Refrigerant leaving the evaporator and condenser is saturated.
- The frictional pressure drops in the pipes, mixer, and GAX heat exchangers are neglected.
- The output streams from the generator and the absorber are in equilibrium.
- The approach temperature at the ends of the GAX heat exchanger is zero.

3.1 | Thermodynamic analysis

The mass balance equation for a piece of equipment as a steady-state control volume is:

$$\sum_i \dot{m}_i = \sum_e \dot{m}_e. \quad (1)$$

The conservation of ammonia mass in the GAX cycle is defined:

$$\sum_i \dot{m}_i x_i = \sum_e \dot{m}_e x_e. \quad (2)$$

The energy balance for a steady-state control volume is written considering the first law of thermodynamics:

$$\dot{Q} - \dot{W} = \sum_e \dot{m}_e h_e - \sum_i \dot{m}_i h_i. \quad (3)$$

The exergy destruction rate for a piece of equipment is expressed²³:

$$\dot{E}x_D = \sum_j \left(1 - \frac{T_0}{T_j}\right) \dot{Q}_j - \dot{W} + \sum_i \dot{E}x_i - \sum_e \dot{E}x_e. \quad (4)$$

The distinction between energy and exergy balance terms is revealed by comparing Equations (3) and (4). It is universally known that energy is not destroyed or created. It only changes form through a process. On the other hand, exergy is a destroyable parameter and is conserved just in reversible processes. Hence, exergy analysis can be helpful for detecting the sources and extent of energy loss and irreversibilities in a thermodynamic system and improving the efficiency of the processes.

The total exergy of a stream is composed of physical and chemical exergy terms if potential and kinetic exergies are neglected:

$$\dot{E}x = \dot{E}x_{\text{ch}} + \dot{E}x_{\text{ph}}. \quad (5)$$

The physical and chemical exergies are determined respectively as²³:

$$\dot{E}x_{\text{ph}} = \dot{m}[(h - h_0) - T_0(s - s_0)], \quad (6)$$

$$\dot{E}x_{\text{ch}} = \frac{\dot{m}}{MW_{\text{mix}}} \sum_k y_k \bar{e}_k^{\text{ch}} + \bar{R}T_0 \sum_k y_k \ln y_k, \quad (7)$$

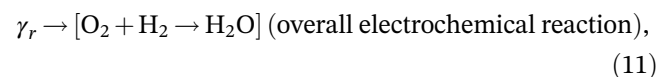
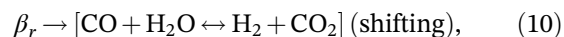
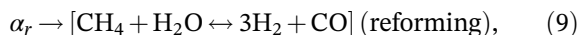
where \bar{e}^{ch} is the standard molar chemical exergy.

The chemical exergy for the ammonia-water mixture can be calculated as²³:

$$\dot{E}x_{\text{ch}} = \dot{m} \left[\left(\frac{x}{MW_{\text{NH}_3}} \right) \bar{e}_{\text{NH}_3}^{\text{ch}} + \left(\frac{1-x}{MW_{\text{water}}} \right) \bar{e}_{\text{water}}^{\text{ch}} \right]. \quad (8)$$

3.2 | SOFC electrochemical modeling

Following reactions take place in an SOFC stack with internal reforming of methane²⁴:



α_r , β_r , and γ_r are conversion rates for Equations (9) to (11), respectively. The water-gas shifting (WGS) and electrochemical reactions are exothermic, but the reforming reaction is endothermic. So, the internal reforming of methane equilibrates the temperature distribution in the fuel cell stack by consuming a part of the generated heat, which means less cooling load and cost for an internal reforming fuel cell. The necessary steam for the shifting and reforming reactions is provided by recirculating a section of the anode outlet. However, it is important to keep the SOFC steam to carbon ratio in a specific range since lower values of this parameter lead to carbon deposition and catalyst deactivation, which is undesirable. Steam to carbon ratio is calculated as:

$$r_{sc} = \frac{\dot{n}_{H_2O,11}}{\dot{n}_{CH_4,4} + \dot{n}_{CO,11}}. \quad (12)$$

Faraday's law can determine γ_r ²⁵:

$$\gamma_r = \frac{j_{SOFC} N_{cell} A_{act}}{2F}. \quad (13)$$

The equilibrium constants for shifting and reforming reactions are defined as²:

$$K_{Reforming} = \frac{y_{CO} y_{H_2}^3}{y_{CH_4} y_{H_2O}} \left(\frac{P}{P_0} \right)^2 = \exp \left(-\frac{\Delta \bar{g}_{Reforming}^0}{\bar{R} T_{SOFC}} \right), \quad (14)$$

$$K_{Shifting} = \frac{y_{CO_2} y_{H_2}}{y_{CO} y_{H_2O}} = \exp \left(-\frac{\Delta \bar{g}_{Shifting}^0}{\bar{R} T_{SOFC}} \right). \quad (15)$$

Hydrogen is never fully consumed in the SOFC. Fuel utilization factor is calculated to control hydrogen consumption rate:

$$u_f = \frac{\gamma_r}{3\alpha_r + \beta_r + \dot{n}_{H_2,1}}. \quad (16)$$

The molar flow rate of the SOFC outlets can be calculated by applying mass conservation law to the SOFC stack as a control volume. The power production rate of the SOFC stack is determined as:

$$\dot{W}_{SOFC} = j_{SOFC} N_{cell} A_{act} V_{cell,SOFC}. \quad (17)$$

$V_{cell,SOFC}$ is the SOFC stack output voltage. The necessary formulas for calculating the fuel cell voltage are given in Table 1.

3.3 | PEM electrolyzer

A part of the generated power in the SOFC sub-system is consumed in the electrolyzer to split water and produce hydrogen. The total required energy for the electrolysis process is:

$$\Delta H = \Delta G + T \Delta S, \quad (18)$$

ΔG is Gibb's free energy, and $T \Delta S$ is the necessary thermal energy for the water splitting reaction.

The generated hydrogen flow rate is calculated as²⁶:

$$\dot{n}_{H_2,30} = \frac{J_{PEME}}{2F} = \dot{n}_{H_2O,reacted}. \quad (19)$$

Oxygen production rate is as:

$$\dot{n}_{O_2,19} = \frac{J_{PEME}}{4F}. \quad (20)$$

The necessary electrical energy for the electrolysis is the same as its electrical exergy:

$$\dot{W}_{PEME} = \dot{E}x_{PEME} = J_{PEME} V_{cell,PEME}. \quad (21)$$

$V_{cell,PEME}$ is the PEME voltage, and its related equations are listed in Table 1.

3.4 | Performance criteria of the overall system

The net power production rate, cooling capacity, input energy, and heating production rate of the proposed system are defined as:

$$\dot{W}_{net} = \dot{W}_{SOFC} - \dot{W}_{Comp,1} - \dot{W}_{Comp,2} - \dot{W}_{PEME} - \dot{W}_p, \quad (22)$$

$$\dot{Q}_{evap} = \dot{m}_{48} h_{48} - \dot{m}_{49} h_{49}, \quad (23)$$

$$\dot{Q}_{in} = \dot{m}_1 LHV_{CH_4}, \quad (24)$$

$$\dot{Q}_{heating} = \dot{m}_{16} (h_{16} - h_{17}). \quad (25)$$

The power consumption in the GAX cycle pump can be ignored due to its small amount.

The coefficient of performance (COP) of the GAX cycle can be expressed as:

$$COP = \frac{\dot{Q}_{evap}}{\dot{Q}_{gen} + \dot{W}_p}. \quad (26)$$

The energy and exergy efficiencies of the overall system are:

$$\eta = \frac{\dot{W}_{net} + \dot{Q}_{evap} + \dot{m}_{22} LHV_{H_2} + \dot{Q}_{heating}}{\dot{m}_1 LHV_{CH_4}}, \quad (27)$$

$$\psi = \frac{\dot{W}_{net} + \dot{E}x_{48} - \dot{E}x_{49} + \dot{n}_{22} \bar{e}_{H_2}^{ch} + \dot{E}x_{16} - \dot{E}x_{17}}{\dot{n}_1 \bar{e}_{CH_4}^{ch}}. \quad (28)$$

Exergy destruction ratio is the share of a component in the overall system exergy destruction:

TABLE 1 Electrochemical equations of SOFC and proton exchange membrane electrolyzer

Equations	SOFC voltage equations ²⁷⁻²⁹	PEME voltage equations ³⁰
Output voltage	$V_{\text{cell,SOFC}} = V_N - V_{\text{ohm}} - V_{\text{con,a}} - V_{\text{con,c}} - V_{\text{act,a}} - V_{\text{act,c}}$	$V_{\text{cell,PEME}} = V_N + V_{\text{act,c}} + V_{\text{act,a}} + V_{\text{ohm}}$
Nernst voltage	$V_N = -\frac{\Delta G^0}{2F} + \frac{\bar{R}T_{\text{SOFC}}}{2F} \ln\left(\frac{P_{\text{H}_2}\sqrt{P_{\text{O}_2}}}{P_{\text{H}_2\text{O}}}\right)$	$V_N = 1.229 - 8.5 \times 10^{-4}(T_{\text{PEME}} - 298)$
Ohmic overpotential	$V_{\text{ohm}} = (R_C + \sum_i \rho_i L_i) j_{\text{SOFC}}$ $\rho_{\text{el}} = \left(\frac{3.34 \times 10^4}{T_{\text{SOFC}}} \exp\left(-\frac{10300}{T_{\text{SOFC}}}\right)\right)^{-1}, L_{\text{el}} = 0.001 \times 10^{-4} \text{ m}$ $\rho_a = \left(\frac{95 \times 10^6}{T_{\text{SOFC}}} \exp\left(-\frac{1150}{T_{\text{SOFC}}}\right)\right)^{-1}, L_a = 0.05 \times 10^{-4} \text{ m}$ $\rho_c = \left(\frac{42 \times 10^6}{T_{\text{SOFC}}} \exp\left(-\frac{1200}{T_{\text{SOFC}}}\right)\right)^{-1}, L_c = 0.005 \times 10^{-4} \text{ m}$ $\rho_{\text{int}} = \left(\frac{9.3 \times 10^6}{T_{\text{SOFC}}} \exp\left(-\frac{1100}{T_{\text{SOFC}}}\right)\right)^{-1}, L_{\text{int}} = 0.3 \times 10^{-4} \text{ m}$ $R_C = 0$	$V_{\text{ohm}} = J_{\text{PEME}} R_{\text{PEME}}$ $R_{\text{PEME}} = \int_0^D \frac{dx}{\sigma_{\text{PEME}} \lambda(x) }$ $\sigma_{\text{PEME}} \lambda(x) = (0.5139 \lambda(x) - 0.326) \exp\left(1268 \left(\frac{1}{303} - \frac{1}{T_{\text{PEME}}}\right)\right)$ $\lambda_a = 14, \lambda_c = 10, D = 50 \mu\text{m}$
Anode activation overpotential	$V_{\text{act,a}} = \frac{\bar{R}T_{\text{SOFC}}}{F} \left(\sinh^{-1}\left(\frac{j_{\text{SOFC}}}{2j_{0,a}}\right)\right), j_{0,s} = 6500 \text{ A/m}^2$	$V_{\text{act,a}} = \frac{\bar{R}T_{\text{PEME}}}{F} \sinh^{-1}\left(\frac{J_{\text{PEME}}}{2j_{0,a}}\right)$ $J_{0,a} = J_{\text{ref,a}} \exp\left(-\frac{E_{\text{act,a}}}{RT_{\text{PEME}}}\right)$ $E_{\text{act,a}} = 76 \text{ kJ/mol}, J_{\text{ref,a}} = 1.7 \times 10^5 \text{ A/m}^2$
Cathode activation overpotential	$V_{\text{act,c}} = \frac{\bar{R}T_{\text{SOFC}}}{F} \left(\sinh^{-1}\left(\frac{j_{\text{SOFC}}}{2j_{0,c}}\right)\right), j_{0,c} = 2500 \text{ A/m}^2$	$V_{\text{act,c}} = \frac{\bar{R}T_{\text{PEME}}}{F} \sinh^{-1}\left(\frac{J}{2j_{0,c}}\right)$ $J_{0,c} = J_{\text{ref,c}} \exp\left(-\frac{E_{\text{act,c}}}{RT_{\text{PEME}}}\right)$ $E_{\text{act,c}} = 18 \text{ kJ/mol}$ $J_{\text{ref,c}} = 4.6 \times 10^3 \text{ A/m}^2$
Anode concentration overpotential	$V_{\text{con,a}} = \frac{\bar{R}T_{\text{SOFC}}}{2F} \left(\ln\left(1 + \frac{P_{\text{H}_2} \times j_{\text{SOFC}}}{P_{\text{H}_2\text{O}} \times j_{0,a}} - \ln\left(1 - \frac{j_{\text{SOFC}}}{j_{0,a}}\right)\right)\right)$ $j_{s,a} = \frac{2FP_{\text{H}_2} D_{\text{eff,a}}}{\bar{R}T_{\text{SOFC}} L_a}, D_{\text{eff,a}} = 0.2 \times 10^{-4} \text{ m}^2/\text{s}$	-
Cathode concentration overpotential	$V_{\text{con,c}} = -\left(\frac{\bar{R}T_{\text{SOFC}}}{4F} \cdot \ln\left(1 - \frac{j_{\text{SOFC}}}{j_{0,c}}\right)\right)$ $j_{s,c} = \frac{4FP_{\text{O}_2} D_{\text{eff,c}}}{\left(\frac{P_{\text{O}_2}}{P}\right) \bar{R}T_{\text{SOFC}} L_c}, D_{\text{eff,c}} = 0.05 \times 10^{-4} \text{ m}^2/\text{s}$	-

$$Y_{D,k} = \frac{\dot{E}x_{D,k}}{\dot{E}x_{D,T}} \quad (29)$$

The unit emission of carbon dioxide is determined as the ratio of emitted carbon dioxide to the production rate of the system and is used as an environmental performance index:

$$\text{EMI}_{\text{CO}_2} = \frac{\dot{m}_{18}}{\dot{W}_{\text{net}} + \dot{Q}_{\text{evap}} + \dot{m}_{22} \text{LHV}_{\text{H}_2} + \dot{Q}_{\text{heating}}} \times 3600. \quad (30)$$

3.5 | Optimization

After a complete parametric study, the genetics algorithm finds the optimum operating conditions for the maximum exergy efficiency. The Genetic Algorithm (GA) method in EES software is selected for the optimization. In Table 2, necessary parameters for the genetic algorithm are listed.

TABLE 2 Tuning parameters for the genetic algorithm

Parameter	Value
Population size	100
Generation number	500
Probability of crossover	85%
Selection process	Tournament
Tournament size	2

3.6 | Validation

As mentioned before, the proposed system in this work is a new combination of the SOFC sub-system, the GAX cycle, and the PEME unit. So, if each sub-system is validated, it can be ensured that the developed model for the overall system is accurate.

- *SOFC sub-system:* The data of Tao et al³¹ are utilized to validate the SOFC electrochemical modeling. In Table 3, the calculated fuel cell voltages in this work for several current densities are compared with those

TABLE 3 Validation of the SOFC electrochemical by Reference 31

j_{SOFC} (A/m^2)	$V_{\text{cell,SOFC}}$ (V) (Tao et al ³¹)	$V_{\text{cell,SOFC}}$ (V) (Present work)
2000	0.76	0.76
3000	0.68	0.72
4000	0.62	0.68
5000	0.57	0.64
6000	0.52	0.60

Note: $T_{\text{SOFC}} = 1100 \text{ K}$, $u_f = 0.85$.

in Reference 31. As Table 3 indicates, these two results have a good agreement.

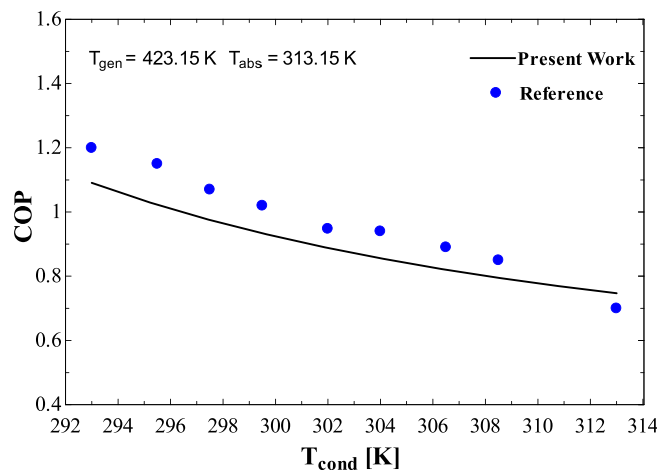
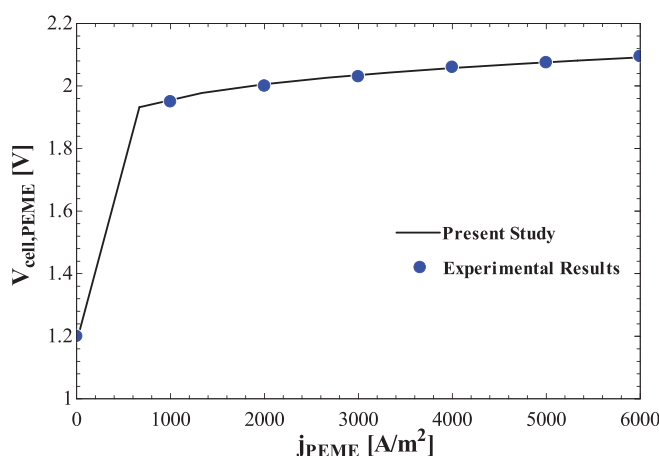
- *GAX absorption refrigeration cycle*: The results of Kumar et al²² are selected to verify the simulation of the GAX cycle. Figure 2 shows the results of this article and those in Reference 22. In this figure, the effect of varying the condenser temperature on the cycle's coefficient of performance is depicted. Accordingly, there is a good agreement between the results, and the maximum absolute error is 8%.
- *PEME unit*: The experimental results available by Leung et al³² are considered to validate the PEME unit modeling code. Figure 3 demonstrates the effect on the PEME Voltage of its current density for the present work and Reference 32. As demonstrated in Figure 3, there is a good match between the results, and the maximum absolute error is 5%.

4 | RESULTS AND DISCUSSION

In this part, the system is studied from the energy, exergy, and environmental viewpoints. The effects of changing main operating parameters, that is, fuel utilization factor, fuel cell current density, generator temperature, condenser temperature, evaporator temperature, and steam to carbon ratio, on the system performance are also investigated. After that, the best values of key parameters for obtaining the maximum exergy efficiency are determined by applying the genetic algorithm. Necessary input data for solving modeling equations of the system at the base case are listed in Table 4.

4.1 | Parametric study

The effect on the system performance of the fuel utilization factor is depicted in Figure 4 for two values of the evaporator temperature. As shown in Figure 4A, at a

**FIGURE 2** The influence of the condenser temperature on the GAX cycle's COP**FIGURE 3** Validation of the PEME modeling

constant evaporator temperature, when the fuel utilization factor increases from 0.7 to 0.88, the net power, cooling, and heating production rates decrease 25.61%, 20.03%, and 20.06%, respectively. Higher fuel utilization factor leads to the lower fuel and air inputs and a lower mass flow rate in the components. Hence, the SOFC-generated power, the available heat for the GAX cycle, and hot water production decrease. With the same justification, as shown in Figure 4B, the input energy and total exergy destruction rate reduce by 10.27% and 14.87%, respectively. However, since the operating parameters of the electrolyzer are constant, changing the fuel utilization factor or the evaporator temperature does not affect the hydrogen production rate. Figure 4C shows that the energy and exergy efficiencies first increase to their maximum and, after that, decrease by further increasing the fuel utilization factor. On the other hand, the unit CO_2 emission has a minimum value at a specific value of u_f .

TABLE 4 Input data for modeling the proposed multigeneration system^{13,32}

Parameter	Symbol	Value
Fuel cell active surface area	A_{act} (m ²)	0.01
Temperature difference along the SOFC stack	ΔT_{SOFC}	100
Inverter efficiency	η_{inv} (%)	95
Compressor isentropic efficiency	$\eta_{comp,1}, \eta_{comp,2}$ (%)	85
Pump isentropic efficiency	η_p (%)	50
Heat exchanger efficiency	ε_{HX} (%)	80
Pressure loss in SOFC stack	ΔP_{SOFC} (%)	2
Pressure loss in afterburner	ΔP_{AB} (%)	2
Pressure loss in heat exchangers	ΔP_{HX} (%)	2
Fuel utilization factor	u_f	0.79
Generator temperature	T_{gen} (K)	438.15
Condenser temperature	T_{cond} (K)	308.15
Evaporator temperature	T_{evap} (K)	278.15
Steam to carbon ratio	r_{sc}	2
PEME unit operating temperature	T_{PEME} (K)	353.15
PEME current density	j_{PEME} (A/m ²)	2000
Number of cells	N_{cell}	11 000
Pressure ratio for compressors	r_p	1.1
Degassing range	D_x	0.3
SOFC stack current density	j_{SOFC} (A/m ²)	6500

This optimum point occurs at $u_f = 0.798$ for the base case condition. This trend is justifiable if Figure 4A,B and Equations (27) and (28) are considered. When the fuel utilization factor increases from 0.7 to 0.798, the reduction rate of the input energy overcomes the decreasing rate of the system's valuable products. Hence, the system efficiencies increase, and EMI_{CO_2} decreases. After that point, the reverse effect is established.

Referring to Figure 4A, it is evident that increasing the evaporator temperature has a positive effect on the cooling production rate because a higher evaporator temperature means more mass flow rate in the GAX cycle. But it slightly decreases the system heating production rate. It should be highlighted that the GAX cycle parameters do not influence the system's net power production, the input energy, and the hydrogen production rate because it is a bottoming cycle. As depicted in Figure 4B, the total exergy destruction rate increases when the evaporator temperature increases from 275.15 K to 288.15 K due to the GAX cycle exergy destruction. According to Figure 4C, the energy efficiency increases, and EMI_{CO_2} decreases because of the system's higher cooling rate.

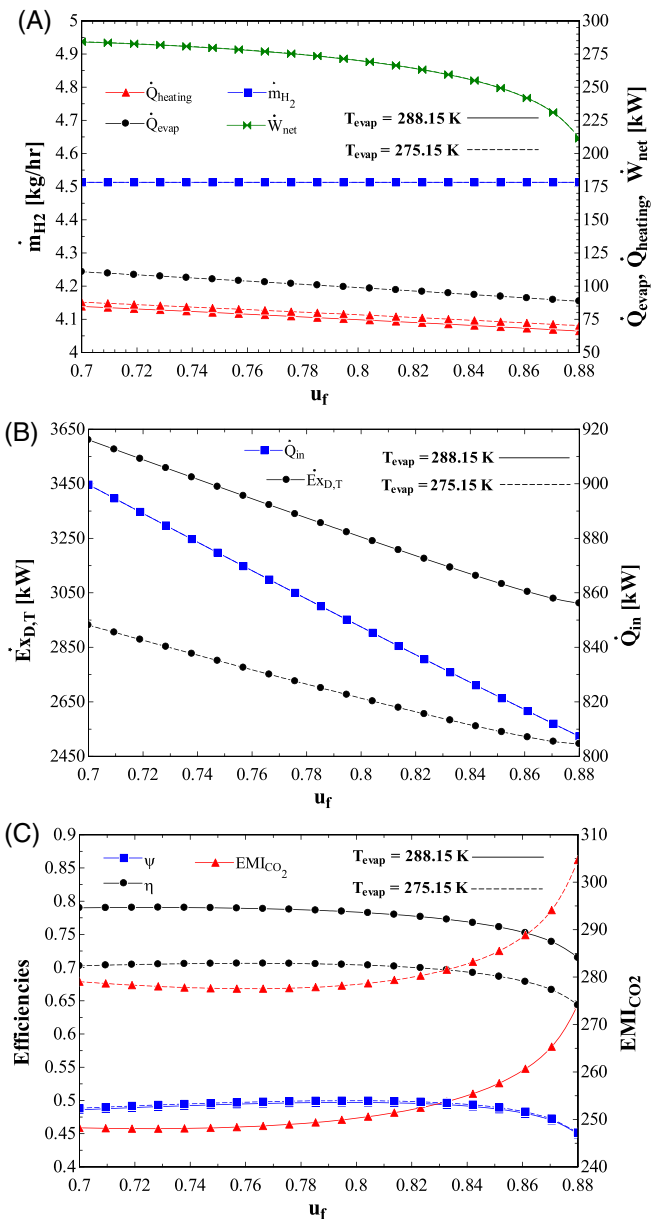


FIGURE 4 The effect on the system performance of fuel utilization factor at different evaporator temperatures: (A) system's products, (B) input energy and total exergy destruction, and (C) system efficiencies and environmental performance

However, the exergy efficiency decreases as a result of the reduction in the heating production rate.

Figure 5 demonstrates the effect of changing SOFC current density and generator temperature on the overall system performance. Referring to Figure 5A,B, as the current density increases from 2000 to 8000 A/m², the power production rate increases from 20.9 to 317.8 kW, and the input energy from 260.9 to 1050 kW. Also, the cooling capacity and heating production rate increase linearly. In fact, at constant fuel utilization factor and generator temperature, higher current density demands more air and

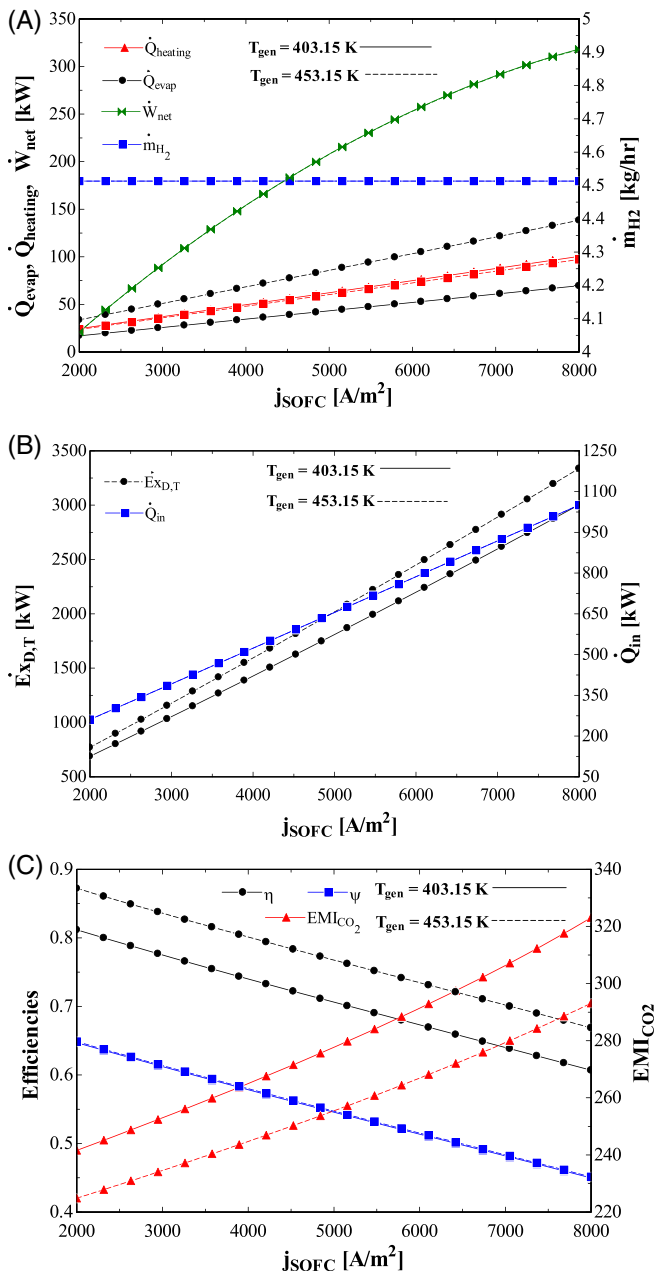


FIGURE 5 The effect of fuel cell current density on the system performance at different generator temperatures: (A) system's products, (B) input energy and total exergy destruction, and (C) system efficiencies and environmental performance

fuel flow rates. Also, SOFC-generated power and the input heat of the GAX cycle increase. However, according to Figure 5B, the destructed exergy of the components has an increasing trend due to the increased flow rate in the system. As Figure 5C shows, the increase of the input energy harms the system efficiencies and makes them decrease by about 20%. Additionally, unit emission of carbon dioxide rises as the current density increases, mostly due to the rise in the rate of emitted carbon dioxide.

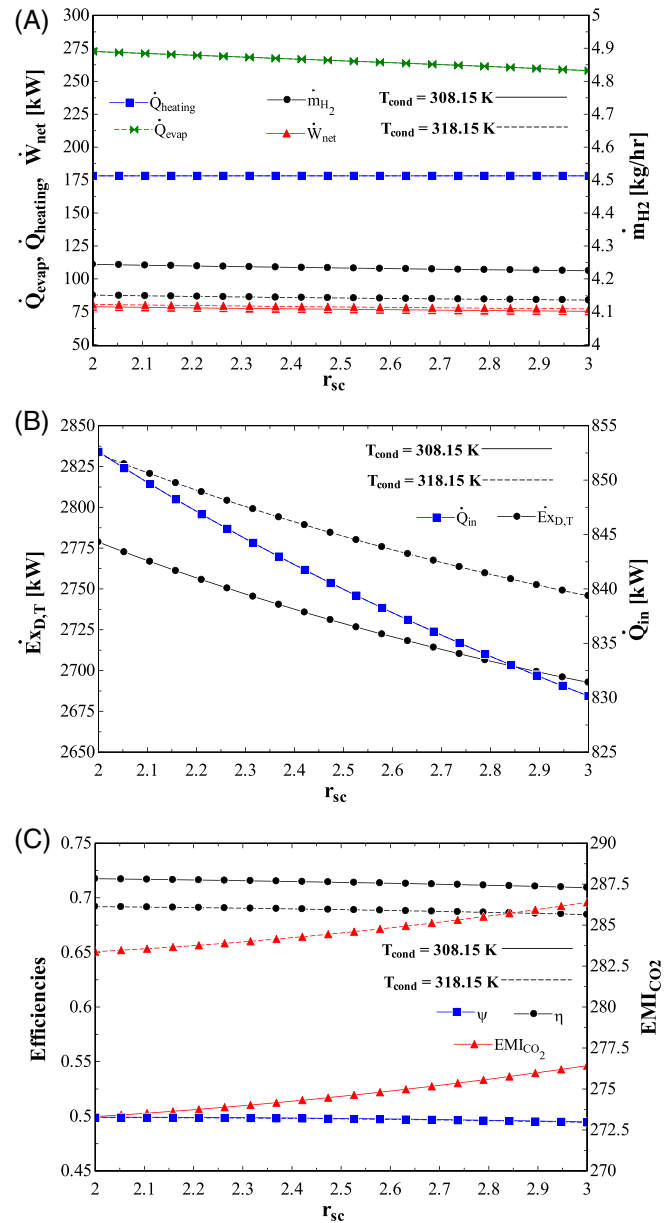


FIGURE 6 The effect of steam to carbon ratio on the system performance at different condenser temperatures: (A) system's products, (B) input energy and total exergy destruction, and (C) system efficiencies and environmental performance

At a constant value of the SOFC current density, higher generator temperature leads to a higher flow rate in the GAX cycle and higher cooling production rate in the evaporator, as in Figure 5A. On the other hand, hot water production slightly decreases. As depicted in Figure 5B, a higher mass flow rate in the GAX cycle leads to the higher total exergy destruction. Also, as depicted in Figure 5C, higher energy and exergy efficiencies and lower EMI_{CO_2} are achieved at higher generator temperature.

Steam to carbon ratio and condenser temperature are other parameters whose influence on the system behavior is investigated in Figure 6. As evident in Figure 6A, increasing the steam to carbon ratio harms the net power production, heating production, and cooling effect. Since higher steam to carbon ratio means lower electrochemical conversion and inlet fuel; thus, SOFC power generation rate, total exergy destruction, and inlet energy decrease. The cathode outlet flow rate and the supplied heat for the GAX cycle also decrease. The overall effect, as shown in Figure 6C, is the slight reduction in the system efficiencies. The decrease of useful exergy due to the steam to carbon ratio increment leads to higher unit CO₂ emission.

If the steam to carbon ratio is kept constant and the condenser temperature increases from 308.15 K to 318.15 K, the cooling load in the evaporator decreases, but the heating rate decreases. Furthermore, as shown in Figure 6B, higher amounts of total exergy destruction are obtained for higher values of the condenser temperature. Finally, energy efficiency decreases by increasing the condenser temperature, EMI_{CO2} increases, but the exergy efficiency is unchanged.

The obtained results in Figures 4 to 6 demonstrate that the environmental and thermodynamic behaviors of the proposed overall system are in the same direction. In other words, any changes in the operating parameters for enhancing the system energy and exergy efficiencies also lead to better environmental performance. Moreover, changing the GAX parameters affect the energy efficiency more than the exergy efficiency. This can be justifiable as the exergy content of the system products is considered in the exergy efficiency calculations.

4.2 | Optimization results

The parametric study in the previous section reveals that the following parameters are essential for optimizing the system exergy efficiency: steam to carbon ratio, fuel utilization factor, SOFC current density, evaporator temperature, condenser temperature, and generator temperature. The aim is to maximize exergy efficiency through the genetic algorithm. The parameters mentioned above are considered as the decision variables with the following bounds:

$$2000 \frac{\text{A}}{\text{m}^2} \leq j_{\text{SOFC}} \leq 8000 \frac{\text{A}}{\text{m}^2}$$

$$2 \leq r_{\text{sc}} \leq 3$$

$$0.7 \leq u_f \leq 0.9$$

$$413.15 \text{ K} \leq T_{\text{gen}} \leq 453.15 \text{ K}$$

$$303.15 \text{ K} \leq T_{\text{cond}} \leq 318.15 \text{ K}$$

$$275.15 \text{ K} \leq T_{\text{evap}} \leq 288.15 \text{ K}$$

The optimization and base-case results are summarized in Table 5. The maximum exergy efficiency and its related energy efficiency are about 14.5% higher than the corresponding values for the base case. Also, the net generated power, cooling load, heating production rate, total exergy destruction rate, input energy, and unit carbon dioxide emission are 45.38, 39.35, 27.18, 844.8, 302.7 kW, and 227.3, respectively, all of them are lower compared to those for the base case.

TABLE 5 System performance at base case vs optimum case

Parameters	Base case	Optimal case
$j_{\text{SOFC}} \left(\frac{\text{A}}{\text{m}^2}\right)$	6500	2333
$u_f (-)$	0.79	0.815
$r_{\text{sc}} (-)$	2	2
$T_{\text{gen}} (\text{K})$	438.15	451.25
$T_{\text{cond}} (\text{K})$	308.15	304.26
$T_{\text{evap}} (\text{K})$	278.15	276.539
$\dot{W}_{\text{net}} (\text{kW})$	272.6	45.38
$\dot{Q}_{\text{evap}} (\text{kW})$	111	39.35
$\dot{Q}_{\text{heating}} (\text{kW})$	78.91	27.18
$\dot{E}X_{\text{D,T}} (\text{kW})$	2779	844.8
$\dot{Q}_{\text{in}} (\text{kW})$	852.6	302.7
η	0.7174	0.8625
Ψ	0.4992	0.6443
EMI _{CO2}	273.3	227.3
$\dot{m}_{\text{H}_2} \left(\frac{\text{kg}}{\text{hr}}\right)$	4.513	4.513

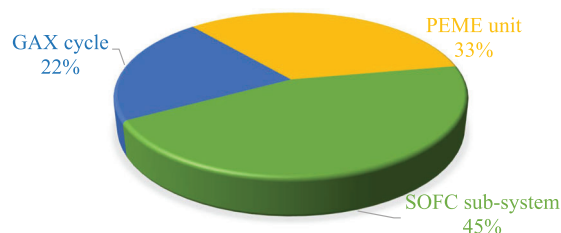


FIGURE 7 The exergy destruction ratio of SOFC, GAX, and PEME sub-system

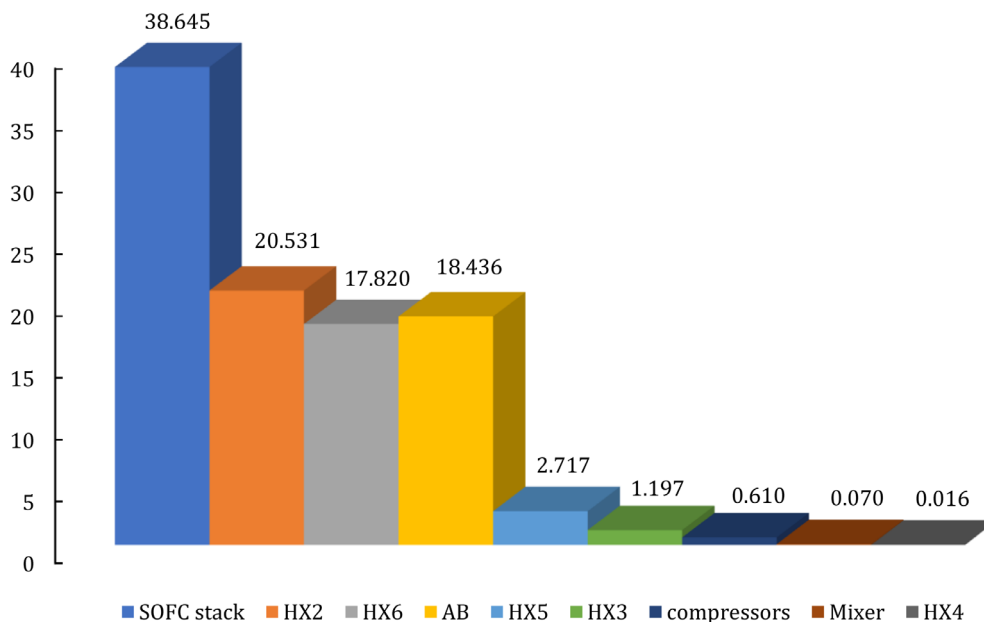


FIGURE 8 The exergy destruction rate of the SOFC components

Figure 7 demonstrates the exergy destruction ratio of each sub-system at the optimal case. The SOFC has the major share in the total exergy destruction rate, almost 45%, because it contains the greatest number of components and all sources of irreversibility, that is, mixing, finite temperature difference heat transfer, reaction, and combustion. The second highest exergy destruction ratio belongs to the PEME unit, 33% of the total irreversibility. On the other hand, the GAX cycle has a minor contribution to the overall system irreversibility due to its small size and lack of the reaction process.

The detailed distribution of the exergy destruction in the SOFC sub-system is illustrated in Figure 8. According to this figure, the SOFC stack, HX2, the afterburner, and HX6 own the highest irreversibility ratios in the SOFC sub-system.

The temperature, pressure, and flow rate of the streams at the optimal case are listed in Table 6. Finally, the proposed system is compared to other multi-generation systems in Table 7, indicating the improved performance of our proposed system.

5 | CONCLUSIONS

In this work, a new integrated SOFC-GAX-PEME system for simultaneous generation of electric power, cooling, heating, and hydrogen is designed, and its thermodynamic and environmental performances are studied completely. The waste heat and streams of the SOFC sub-system are recovered in other cycles, and hence, the overall system efficiency enhances. The thermodynamic and environmental behavior of the system is modeled by applying

energy, exergy, and environmental relations. Then, the parametric study is accomplished to reveal the effect of the key variables on the system performance. After that, the exergetic performance of the system is optimized by applying the genetic algorithm. The important results of the present study can be mentioned as follows:

- Although increasing fuel cell current density from 2000 to 8000 A/m² leads to higher values of system products, it deteriorates thermodynamic efficiencies and environmental performance due to the increase of input fuel flow rate.
- As the fuel utilization factor increases from 0.7 to 0.88, the net power production rate, heating generation, and cooling capacity decrease by 25.61%, 20.06%, and 20.03%, respectively. Moreover, there is a 10.27% decrease in the system input energy and a 14.87% decrease in the total exergy destruction rate.
- There is a specific value of fuel utilization factor in which energy and exergy efficiencies are maximized, and unit CO₂ emission is minimized.
- Increasing the steam to carbon ratio has a negative effect on the system efficiencies. However, unit CO₂ emission has a direct relationship with steam to carbon ratio.
- Higher thermodynamic efficiencies, better environmental performance, and more cooling load can be achieved at higher values of the generator temperature.
- When the evaporator temperature rises from 275.15 K to 288.15 K, the total exergy destruction rate and energy efficiency also increase, but EMI_{CO₂} and the exergy efficiency decrease.
- Changing the condenser temperature does not affect the exergy efficiency. However, when it increases from

TABLE 6 Streams' conditions

St. No.	1	2	3	4	5	6	7	8	9
Flow rate (kmol/hr)	1.337	1.337	1.337	6.646	55.116	55.116	55.116	52.74	9.32
Temperature (K)	298.2	305.9	449.9	762.4	298.2	307.8	762.4	862.4	862.4
Pressure (bar)	1	1.1	1.078	1.078	1	1.1	1.078	1.056	1.056
St. No.	10	11	12	13	14	15	16	17	18
Flow rate (kmol/hr)	4.01	5.31	4.427	52.74	52.74	4.427	4.427	4.427	1.337
Temperature (K)	862.4	862.4	1105	478.6	423.4	886.7	751.04	501.19	373.2
Pressure (bar)	1.056	1.056	1.035	1.035	1.015	1.015	1.015	1.013	1.007
St. No.	19	20	21	22	23	24	25	26	27
Flow rate (kmol/hr)	3.09	5.31	3.054	2.256	2.22	0.417	0.417	0.02142	0.02142
Temperature (K)	373.2	373.2	373.2	373.2	373.2	373.2	682.4	338.8	339.2
Pressure (bar)	1.007	1.007	1.007	1.007	1.007	1.007	1.001	4.514	12
St. No.	28	29 L	29 V	30	31	32 L	32 V	33	34
Flow rate (kmol/hr)	0.02142	0.01836	0.00391	0.01456	0.01456	0.01769	0.00322	0.00065	0.00761
Temperature (K)	376.2	414.2	414.2	451.3	414.2	376.2	376.2	376.3	376.2
Pressure (bar)	12	12	12	12	4.514	4.514	4.514	12	12
St. No.	35	36	37	38	39	40	41	42	43
Flow rate (kmol/hr)	0.007	0.007	0.007	0.007	0.007	0.007	0.02119	0.02119	0.02119
Temperature (K)	334.1	304.3	282.2	274.6	276.5	293.2	298.2	369.2	494.2
Pressure (bar)	12	12	12	4.514	4.514	4.514	1	1	1
St. No.	44	45	46	47	48	49			
Flow rate (kmol/hr)	0.00666	0.00666	0.06736	0.06736	0.09826	0.09826			
Temperature (K)	298.2	369.2	298.2	327.1	298.2	279.6			
Pressure (bar)	1	1	1	1	1	1			

TABLE 7 Benefits and downsides of the proposed quadruple-generation system vs other multigeneration systems

Case study	System type/prime mover	Fuel/fuel processing type	Application	Efficiencies
Present work	Multigeneration system/ SOFC-GAX-PEME	Methane	Cooling, heating, and hydrogen besides power production	$\eta \approx 84\%$ $\psi \approx 65\%$
You et al ⁸	Micro poly-generation / SOFC-MGT-MED	Methane	Power, cooling, heating, and freshwater	$\eta \approx 64.7\%$ $\psi \approx 62.4\%$
Siddiqui et al ³³	SOFC-GT/ammonia fuel cell	Methane/solar power	power, hydrogen, cooling, and hot water	$\eta \approx 39.1\%$ $\psi \approx 38.7\%$
Chitgar et al ¹¹	SOFC-GT	Methane	electricity, freshwater, and hydrogen	$\eta \approx 64.3\%$ $\psi \approx 49\%$
Peng et al ¹⁷	SOFC-CCHP	Natural gas	Electrical, thermal power, and cooling production	$\eta \approx 70.8\%$ $\psi \approx 50.6\%$
Akrami et al ¹⁸	Multi-generation/SOFC	Solar power	Cooling, electrical, and hydrogen production	$\eta_{\text{Day mode}} \approx 21.24\%$ $\eta_{\text{Night mode}} \approx 35.86\%$
Sadeghi et al ¹⁹	SOFC-GAX-HX	Biomass	Power, cooling, and heating production	$\psi \approx 48.42\%$
Perna et al ²⁰	SOFC-CCHP	Ammonia	Heat, hydrogen, and power	$\eta_{\text{tri,concept1}} \approx 81\%$ $\eta_{\text{tri,concept2}} \approx 71\%$

308.15 K to 318.15 K, higher values of total exergy destruction and EMI_{CO_2} with decreased amounts of the cooling load, the heating rate, and energy efficiency are obtained.

- The single-objective exergy optimization through genetic algorithm indicates that the system energy and exergy efficiencies can be as high as 0.8625 and 0.6443, respectively.
- SOFC sub-system has the largest share (45%) in the overall system exergy destruction rate.
- The fuel cell stack and HX2 contribute the most to the overall system irreversibility with the exergy destruction rates of 38.645 and 20.531 kW, respectively.

NOMENCLATURE

A_{act}	Cell active area (m^2)
AB	Afterburner
Comp	Compressor
COP	Coefficient of performance
D	Electrolyzer membrane thickness (μm)
D_{eff}	Effective gas diffusion factor (m^2/s)
D_x	Degassing range
E	Activation energy (kJ/mol)
EMI	Unit emission of carbon dioxide
EPC	Exergetic performance coefficient
EV	Expansion valve
\dot{E}_x	Exergy rate (kW)
\bar{e}^{ch}	Standard chemical exergy of species (kJ/kmol)
F	Faraday constant (C/kmol)
G	Gibb's free energy (kJ)
GAXA	GAX-absorber
GAXD	GAX-desorber
\bar{g}^0	Molar Gibbs free energy (kJ/kmol)
h	Specific enthalpy (kJ/kg)
H	Enthalpy (kJ)
HX	Heat exchanger
j	Current density (A/m^2)
J	Current (A)
j_0	Exchange current density (A/m^2)
j_s	Limiting current density (A/m^2)
J_{ref}	Pre-exponential factor (A/m^2)
K	Equilibrium constant
L	Thickness (m)
LHV	Lower heating value (kJ/kg)
M	Mixer
\dot{m}	Mass flow rate (kg/s)
MW	Molecular weight (kg/kmol)
\dot{n}	Molar flow rate (kmol/s)
N_{cell}	Number of cells
P	Pressure (bar)
p	Pump
PEM	Proton exchange membrane
\dot{Q}	Heat transfer rate (kW)
\bar{R}	Universal gas constant (kJ/kmol.K)
R_c	Contact resistance

r_p	Pressure ratio
R_{PEM}	Proton exchange member resistance (Ω)
r_{sc}	Steam to carbon ratio
s	Specific entropy (kJ/kg.K)
S	Entropy (kJ/K)
SOFC	Solid oxide fuel cell
T	Temperature (K)
u_f	Fuel utilization factor
V	Voltage (V)
\dot{W}	Power (kW)
x	Ammonia concentration
y	Mole fraction
Y	Exergy destruction ratio

Greek symbols


$\lambda(x)$	Water content at location x in the membrane (Ω^{-1})
η	Energy efficiency
Ψ	Exergy efficiency
ρ	Electrical resistivity
σ_{PEM}	Proton conductivity in PEM (s/m)
α_r	Conversion rate of reforming reaction
β_r	Conversion rate of shifting reaction
γ_r	Conversion rate of electrochemical reaction

Subscripts

0	Environmental condition
1, 2, 3, ...	State point
a	Anode
abs	Absorber
act	Activation
c	Cathode
ch	Chemical
con	Concentration
D	Destruction
e	Outlet
el	Electrode
evap	Evaporator
gen	Generator
i	Inlet
int	Interconnection
inv	DC to AC inventor
k	K_{th} component
loss	Loss
mix	Mixture
N	Nernst
net	Net
ohm	Ohmic
PEME	Proton exchange membrane electrolyzer
ph	Physical

ORCID

Mousa Mohammadpourfard  <https://orcid.org/0000-0002-6098-924X>

Saeed Zeinali Heris  <https://orcid.org/0000-0001-6203-0385>

REFERENCES

- Zaidi SMJ, Rauf MA. Fuel cell fundamentals. *Polymer Membranes for Fuel Cells*; Boston, MA: Springer; 2009:1-6. doi: 10.1007/978-0-387-73532-0_1
- Khani L, Mehr AS, Yari M, Mahmoudi SMS. Multi-objective optimization of an indirectly integrated solid oxide fuel cell-gas turbine cogeneration system. *Int J Hydrog Energy*. 2016;41:21470–21488. doi:10.1016/j.ijhydene.2016.09.023
- Taheri MH, Khani L, Mohammadpourfard M, Aminfar H. Multi-objective optimization of a novel biomass-based multi-generation system consisting of liquid natural gas open cycle and proton exchange membrane electrolyzer. *Int J Energy Res*. 2021;45(11):16806–16823. doi:10.1002/er.6931
- Jia J, Zang G, Paul MC. Energy, exergy, and economic (3E) evaluation of a CCHP system with biomass gasifier, solid oxide fuel cells, micro-gas turbine, and absorption chiller. *Int J Energy Res*. 2021;45(10):15182–15199. doi: 10.1002/er.6794
- Habibollahzade A, Mehrabadi ZK, Houshfar E. Exergoeconomic and environmental optimisations of multi-generation biomass-based solid oxide fuel cell systems with reduced CO₂ emissions. *Int J Energy Res*. 2021;45(7):10450–10477. doi:10.1002/er.6532
- Hosseinpour J, Chitsaz A, Eisavi B, Yari M. Investigation on performance of an integrated SOFC-Goswami system using wood gasification. *Energy*. 2018;148:614–628. doi:10.1016/j.energy.2018.01.162
- Tian M, Yu Z, Zhao H, Yin J. Thermodynamic analysis of an integrated solid oxide fuel cell, organic Rankine cycle and absorption chiller trigeneration system with CO₂ capture. *Energy Convers Manag*. 2018;171:350–360. doi:10.1016/j.enconman.2018.05.108
- You H, Han J, Liu Y, Chen C, Ge Y. 4E analysis and multi-objective optimization of a micro poly-generation system based on SOFC/MGT/MED and organic steam ejector refrigerator. *Energy*. 2020;206:118122. doi:10.1016/j.energy.2020.118122
- Ebrahimi M, Moradpoor I. Combined solid oxide fuel cell, micro-gas turbine and organic Rankine cycle for power generation (SOFC–MGT–ORC). *Energy Convers Manag*. 2016;116:120–133. doi:10.1016/j.enconman.2016.02.080
- Gholamian E, Zare V. A comparative thermodynamic investigation with environmental analysis of SOFC waste heat to power conversion employing Kalina and organic Rankine cycles. *Energy Convers Manag*. 2016;117:150–161. doi:10.1016/j.enconman.2016.03.011
- Chitgar N, Moghimi M. Design and evaluation of a novel multi-generation system based on SOFC-GT for electricity, fresh water and hydrogen production. *Energy*. 2020;197:117162. doi:10.1016/j.energy.2020.117162
- Atsonios K, Samlis C, Manou K, et al. Technical assessment of LNG based polygeneration systems for non-interconnected Island cases using SOFC. *Int J Hydrog Energy*. 2021;46:4827–4843. doi:10.1016/j.ijhydene.2020.03.072
- Khani L, Mahmoudi SMS, Chitsaz A, Rosen MA. Energy and exergoeconomic evaluation of a new power/cooling cogeneration system based on a solid oxide fuel cell. *Energy*. 2016;94:64–77. doi:10.1016/j.energy.2015.11.001
- Zhao H, Jiang T, Hou H. Performance analysis of the SOFC–CCHP system based on H₂O/li–Br absorption refrigeration cycle fueled by coke oven gas. *Energy*. 2015;91:983–993. doi: 10.1016/j.energy.2015.08.087
- Reyhani HA, Meratizaman M, Ebrahimi A, Pourali O, Amidpour M. Thermodynamic and economic optimization of SOFC-GT and its cogeneration opportunities using generated syngas from heavy fuel oil gasification. *Energy*. 2016;107:141–164. doi:10.1016/j.energy.2016.04.010
- Ozcan H, Dincer I. Performance evaluation of an SOFC based trigeneration system using various gaseous fuels from biomass gasification. *Int J Hydrog Energy*. 2015;40:7798–7807. doi: 10.1016/j.ijhydene.2014.11.109
- Peng MY-P, Chen C, Peng X, Marefati M. Energy and exergy analysis of a new combined concentrating solar collector, solid oxide fuel cell, and steam turbine CCHP system. *Sustain Energy Technol Assess*. 2020;39:100713. doi:10.1016/j.seta.2020.100713
- Akrami E, Gholami A, Ameri M, Zandi M. Integrated an innovative energy system assessment by assisting solar energy for day and night time power generation: exergetic and exergoeconomic investigation. *Energy Convers Manag*. 2018;175:21–32. doi:10.1016/j.enconman.2018.08.075
- Sadeghi M, Chitsaz A, Mahmoudi SMS, Rosen MA. Thermoeconomic optimization using an evolutionary algorithm of a trigeneration system driven by a solid oxide fuel cell. *Energy*. 2015;89:191–204. doi:10.1016/j.energy.2015.07.067
- Perna A, Minutillo M, Jannelli E, Cigolotti V, Nam SW, Han J. Design and performance assessment of a combined heat, hydrogen and power (CHHP) system based on ammonia-fueled SOFC. *Appl Energy*. 2018;231:1216–1229. doi:10.1016/j.apenergy.2018.09.138
- Jawahar CP, Saravanan R. Generator absorber heat exchange based absorption cycle—a review. *Renew Sust Energy Rev*. 2010; 14:2372–2382. doi:10.1016/j.rser.2010.05.002
- Kumar AR, Udayakumar M. Studies of compressor pressure ratio effect on GAXAC (generator–absorber–exchange absorption compression) cooler. *Appl Energy*. 2008;85:1163–1172. doi: 10.1016/j.apenergy.2008.03.002
- Kotas TJ. Exergy concepts for thermal plant: first of two papers on exergy techniques in thermal plant analysis. *Int J Heat Fluid Flow*. 1980;2:105–114. doi:10.1016/0142-727X(80) 90028-4
- Amedi HR, Bazooyar B, Pishvaie MR. Control of anode supported SOFCs (solid oxide fuel cells): part I. mathematical modeling and state estimation within one cell. *Energy*. 2015;90: 605–621. doi:10.1016/j.energy.2015.07.095
- Akkaya AV, Sahin B, Huseyin Erdem H. Exergetic performance coefficient analysis of a simple fuel cell system. *Int J Hydrog Energy*. 2007;32:4600–4609. doi:10.1016/j.ijhydene.2007.03.038
- Esmaili P, Dincer I, Naterer GF. Energy and exergy analyses of electrolytic hydrogen production with molybdenum-oxo catalysts. *Int J Hydrog Energy*. 2012;37:7365–7372. doi:10.1016/j.ijhydene.2012.01.076
- Habibollahzade A, Gholamian E, Houshfar E, Behzadi A. Multi-objective optimization of biomass-based solid oxide fuel

- cell integrated with Stirling engine and electrolyzer. *Energy Convers Manag.* 2018;171:1116-1133. doi:10.1016/j.enconman.2018.06.061
28. U.G. Bossel, L. [Dubal, Facts and figures, an International Energy Agency SOFC task report, Switzerland, 1992. <https://www.osti.gov/etdeweb/servlets/purl/7167838>
29. Kim J, Virkar AV, Fung K, Mehta K, Singhal SC. Polarization effects in intermediate temperature, anode-supported solid oxide fuel cells. *J Electrochem Soc.* 1999;146:69-78. doi:10.1149/1.1391566
30. Ahmadi P, Dincer I, Rosen MA. Energy and exergy analyses of hydrogen production via solar-boosted ocean thermal energy conversion and PEM electrolysis. *Int J Hydrog Energy.* 2013;38:1795-1805. doi:10.1016/j.ijhydene.2012.11.025
31. Tao G, Armstrong T, Virkar A. Intermediate Temperature Solid Oxide Fuel Cell Intermediate Temperature Solid Oxide Fuel Cell (IT [IT - -SOFC] Research and Development Activities SOFC) Research and Development Activities at MSRI at MSRI. 2021.
32. Ni M, Leung M, Leung Y. Electrochemistry Modeling of Proton Exchange Membrane (PEM) Water Electrolysis for Hydrogen Production, 2006.
33. Siddiqui O, Dincer I. Analysis and performance assessment of a new solar-based multigeneration system integrated with ammonia fuel cell and solid oxide fuel cell-gas turbine combined cycle. *J Power Sources.* 2017;370:138-154. doi:10.1016/j.jpowsour.2017.10.008

How to cite this article: Khani L, Mohammadpour M, Mohammadpourfard M, Heris SZ, Akkurt GG. Thermodynamic design, evaluation, and optimization of a novel quadruple generation system combined of a fuel cell, an absorption refrigeration cycle, and an electrolyzer. *Int J Energy Res.* 2022;46(6):7261-7276. doi:10.1002/er.7634